American Mineralogist, Volume 59, pages 1083–1093, 1974

Distortions in the Coordination Polyhedra of *M* Site Atoms in Olivines, Clinopyroxenes, and Amphiboles

MICHAEL E. FLEET

Department of Geology, University of Western Ontario, London, Ontario, Canada

Abstract

Distortions resulting from shared edges in the coordination polyhedra of metal (M) site atoms in olivines, $C2/c$ clinopyroxenes and (Ca),Mg,Fe^{2+} amphiboles have been investigated using published crystal structure data. In the clinopyroxenes there is qualitative agreement between the apparent stretching of $M(1)$–$M(1)$ and $M(2)$–Si distances associated with shared polyhedral edges and the calculated relative electrostatic potentials due to the M site atoms. The stretching is attributed to interatomic repulsion and decreases in the sequences, Al > Fe^{3+} > (Cr^{3+}, In) > Mg > Mn^{2+} for $M(1)$ atoms and Ca > Li > Na for $M(2)$ atoms. In Ca amphiboles, in agreement with calculated data, the repulsive force due to Mg is apparently greater than that due to Fe^{2+}. However, in olivines the repulsive force due to Fe^{2+} appears to be greater than that due to Mg.

Although the t_{2g} orbitals on transition metal atoms must project toward octahedral edges, octahedra coordinated about transition metals do not show a consequent reduction in shared-edge-related distortions. Thus, $3d$ electrons in t_{2g} orbitals do not appear to screen the effective atomic charges along M–M and M–Si directions.

In olivines variations with composition of $M(2)$–Si distances, individual M–O bond distances and O–M–O and O–Si–O bond angles indicate slight departures from the linear trends expected for ideal solution.

Introduction

In ferromagnesian minerals the nearest-neighbor octahedra and eight-fold coordinated polyhedra of metal (M) site atoms share edges with each other and, frequently, with the coordination tetrahedra of atoms on adjacent tetrahedral (T) sites. Shared octahedral edges are usually shorter than the ideal values for regular octahedra and, since the corresponding M–M distances are usually greater than the ideal values, this effect is generally attributed to repulsion between the positively charged metal atoms. Pauling (1929) summarized the effects of shared coordination edges on complex ionic crystals in the following rule, "The presence of shared edges, and particularly of shared faces, in a coordinated structure decrease its stability; this effect is large for cations with large valence and small coordination number. . . ." Thus, the repulsion between M atoms related through shared coordination edges should increase with increase in effective atomic charge (Z_{eff}) and with decrease in ionic radius (R). The repulsive force experienced by an M atom from an edge-related M atom must be proportional to the electrostatic potential of the second M atom at the nucleus of the first, which is given by $Z_{\text{eff}}/(M\text{–}M)$, where M–M is the interatomic separation. In general, the effective force due to an M atom coordinated with oxygen must be proportional to the electrostatic potential $Z_{\text{eff}}/(M\text{–O})$.

The dependence of polyhedral distortions in inorganic crystals on simple electrostatic bond characteristics has been supported by Baur (1970). The importance of the repulsion between cations related by shared polyhedral edges was stressed in this study although quantitative estimates of the extent of these repulsions were not attempted.

In the present study on some olivines, clinopyroxenes, and amphiboles, those polyhedral distortions which may be referred to repulsion between edge-related M atoms are outlined, and an attempt is made to correlate the extent of these distortions with estimates of the repulsive forces involved. The aims of this study, then, are quite limited, and full rationalizations of the structural characteristics of these phases will not be attempted. The M atoms considered are Li, Na, and Ca in eight-fold coordinated sites in clinopyroxenes, Al, Fe^{3+}, Cr^{3+}, In, Mg, and Mn^{2+} in octahedral sites in clinopyroxenes, and

Mg and Fe^{2+} in octahedral sites in olivines and amphiboles. The distortions are documented through analysis of specific bond angles and interatomic distances. Estimates of overall polyhedral distortion from variance of polyhedral angles and quadratic elongation (Robinson, Gibbs, and Ribbe, 1971) and from mean-square relative deviations from average bond lengths (Brown and Shannon, 1973) are not suited to the present investigation because repulsive interactions between metal atoms are not the only causes of distortion in the various polyhedra analyzed, and also these interactions are directionally dependent.

There are possible additional complications for edge-related interactions between transition metal atoms. In ideal octahedral coordination, the 3*d* electrons on transition metals will be distributed between the stabilized set of three t_{2g} orbitals and a destabilized set of two e_g orbitals. The e_g orbitals project along the *M*–O directions, toward the ligands, but the t_{2g} orbitals project toward the octahedral edges, that is along the *M*–*M* directions between edge-related *M*-site atoms. With more polarizable ligands ($S^{2-}{}_2$,$As^{2-}{}_2$, and so on) the t_{2g} orbitals extend outward to the extent that attractive, bonding reactions may occur between singly occupied orbitals on edge-related atoms (Fleet, 1973), and repulsive reactions may occur between filled orbitals; for example, in compounds with the marcasite structure interactions between t_{2g} orbitals appear to have been the dominant factors controlling distortions in the coordination octahedra of the metal atoms (Pearson, 1965; Nickel, 1968; Brostigen and Kjekshus, 1970). Although t_{2g} orbitals are assumed to be deeply buried in oxygen coordination polyhedra, electron transfer between overlapping t_{2g} orbitals has been proposed to explain the $Fe^{2+} \rightarrow Fe^{3+}$ charge transfer bands in ferromagnesian silicates (Burns, 1970), and there is a possibility that t_{2g} orbital interactions might be a factor in the distortion of edge-related polyhedra of *M* site atoms. However, these t_{2g} orbitals more likely contribute to the distortions of these polyhedra by screening the nuclear charge on transition metal atoms along the *M*–*M* directions. The screening efficiency of *d* orbitals must have a pronounced angular dependency, and electrons in t_{2g} orbitals, by projecting in *M*–*M* directions, might tend to neutralize the nuclear charge in these directions. This hypothesis can be critically evaluated in the present study.

It should be noted that the high spin 3*d* electron configurations expected for Cr^{3+}, Mn^{2+}, Fe^{2+}, and Fe^{3+} in octahedral coordination with oxygen do not result in unequal electron population of e_g orbitals. Consequently, axial Jahn-Teller distortions are not anticipated in the nearest-neighbor environments of these cations.

Electrostatic Potentials

There has been much discussion in recent years of covalent bonding forces in silicate compounds (for example, Gibbs, Hamil, Bartell, and Yow, 1972; Louisnathan and Gibbs, 1972a, 1972b). Acceptance of a model involving molecular orbitals on the oxygen atoms to account for features in the *T*–O bonds requires that these orbitals must project toward the *M* atoms also, resulting in some degree of orbital overlap in the *M*–O bonds. Thus, the effective charge on a metal atom (Z_{eff}) is less than that indicated by its valence.

An estimate of Z_{eff} may be obtained for any *M* atom from the relationships,

$$Z_{\text{eff}} = iZ,$$

where *i* is the fractional ionic character of the *M*–O bond and *Z* is the ideal ionic charge, and

$$i = 1 - e^{-0.25\Delta X^2} \qquad \text{(Pauling, 1960)},$$

where ΔX is the difference in electronegativity between O^{2-} and *M*. Batsanov (1968) has recommended a revised expression for the relationship between *i* and ΔX, $i = 1 - e^{-0.18\ \Delta X^2}$, which is calibrated against *i* data obtained from the dipole moments of the hydrogen halides. However, the earlier expression, although based on an erroneous *i* value for HF, clearly provides a better fit to the measured *i* data presented by Pauling (1960, Fig. 3–8). Accordingly, values of Z_{eff} (Table 1) have been calculated with electronegativity data from the recent compilation of Batsanov (1968, Table 5) using the original Pauling expression. The resulting values of the electrostatic potential $Z_{\text{eff}}/(M\text{–O})$ for the *M* atoms in octahedral coordination are for ideal *M*–O distances calculated using the data for effective ionic radii of Shannon and Prewitt (1969). These data, used qualitatively, suggest that interatomic *M*–*M* and *M*–*T* repulsion should decrease in the sequence, Al > Cr^{3+} > In $\simeq$ Fe^{3+} = Mg^{2+} > Mn^{2+} > Fe^{2+}. The analogous electrostatic potential data for the eight-fold coordinated *M* site atoms (Table 1) allow the prediction that repulsion with a common *M* or *T* atom should decrease in the sequence Ca > Li > Na.

However, it is well-known that atomic charges calculated from electronegativity data have only approximate significance. This is emphasized by the considerable scatter in the calibration data at high values of ΔX (Pauling, 1960, Fig. 3–8). This calibration is based largely on the dipole moments of gaseous diatomic halide compounds, whereas the present data are for six- and eight-fold oxygen coordinated complexes in solids. Also, no attempt has been made to correct the electronegativity data used for charge effects and hybridization of the oxygen bonding orbitals, and it might be expected by consideration of the electroneutrality principle (Pauling, 1960) that a proportion of the atomic charges would be neutralized by π-bonding. Clearly, before accepting this Z_{eff} data, consideration must be given to charge data obtained by other methods.

A compilation of effective charge data for metal atoms in oxides obtained by a variety of experimental and theoretical methods (Bartenev *et al,* 1972) shows a wide variation. The ranges for the cations included in this study are Mg (1.0 to 1.76), Al (1.23 to 2.43), Mn (1.18 to 1.34), Fe^{2+} (1.03 to 1.32), Fe^{3+} (1.58 to 2.15), and Ca (1.18 to 1.66). The charges from electronegativity data in Table 1 for Mg, Al, Mn, and Ca fall within the respective ranges of the Bartenev *et al* (1972) data but the charges in Table 1 for Fe^{2+} and Fe^{3+} are lower than those reported in their study. Other relevant, comparative charge data are: Mg in $MgSiO_3$ (1.00), Al in various silicates (0.90 to 1.20), and Na in Na_2SiO_3 (0.85), estimated from line shifts in $K\alpha$ X-ray spectra (Urusov, 1967); *M* site atoms of lunar and terrestrial olivines (0.13 to 0.34), by crystal structure refinement with X-ray diffraction data (Wenk and Raymond, 1973); Na in kernite (0.43 to 0.57), by crystal structure refinement with the Extended *L*-shell method (Coppens, 1972); Mg in $MgO^{10-}{}_6$ (1.26) and Al in $AlO^{9-}{}_6$ (1.96), from molecular orbital calculations (Tossell, 1973). Clearly, the data obtained by other methods are fragmentary and do not provide a consistent basis for comparison with the charge data from electronegativities. A partial explanation for the discrepancies in the data must be related to the definition of the charge being measured or calculated in a particular case and the relationship of this charge to the atom involved; for example, Cochran (1961) has cautioned that atomic charges determined from X-ray diffraction may be ambiguous and are dependent on the particular atomic descriptions used.

TABLE 1. Electrostatic Valence Terms

			From Electronegativity Data				Position Method Data	
Metal	Ideal ionic charge (Z)	Effective ionic radius*	Electronegativity (X)	Ionic character of M-O bond (i)	Effective atomic charge (Z_{eff})	Electrostatic potential, $Z_{eff}/(M\text{-}O)$	Effective atomic charge (Z_{eff})	Electrostatic potential $Z_{eff}/(M\text{-}O)$
Mg	+2	0.720	1.2	0.73	+1.5	0.69	+1.14	0.54
Al	+3	0.530	1.6	0.59	+1.8	0.92	+2.43	1.26
Cr	+3	0.615	1.6	0.59	+1.8	0.88		
Mn	+2	0.820	1.4	0.67	+1.3	0.60	+1.18	0.53
Fe	+2	0.770	1.8	0.51	+1.0	0.47	+1.12	0.52
Fe	+3	0.645	1.9	0.47	+1.4	0.69	+2.15	1.05
In	+3	0.790	1.8	0.51	+1.5	0.70		
Li	+1	0.74	1.0	0.79	+0.8	0.37		
Na	+1	1.16	0.9	0.82	+0.8	0.32		
Ca	+2	1.12	1.0	0.79	+1.6	0.63	+1.45	0.58

* Data from Shannon and Prewitt (1969). R(Li^+) for six coordination.

Thus, although the Z_{eff} data used in this study are somewhat crude, an alternative, self-consistent set of charge data covering the range of metal atoms investigated is not available. Self-consistency is an important requirement in such data. The present use of effective charges is purely qualitative, and much more weight is given to the relative order of the electrostatic potential data than to the absolute values of the charges. In this connection, the errors in the Z_{eff} data used are expected to vary systematically within the groups of chemically related polyhedral complexes analyzed. In support of this, independently determined chemical parameters frequently show good correlation with quantities calculated from electronegativity values; for example, binding energies determined by electron spectroscopy for groups of related compounds correlate well with calculated atomic charges (Siegbahn *et al,* 1967).

Finally, Z_{eff} data obtained by an independent method, annihilation of positrons (Bartenev *et al,* 1972), are presented for comparison (Table 1). These data indicate relatively higher charges on Al and Fe^{3+} so that, for octahedrally coordinated *M* atoms, the interatomic repulsion is expected to decrease in the sequence $Al > Fe^{3+} \gg Mg = Mn^{2+} > Fe^{2+}$.

Olivines

In the olivine structure the oxygen atoms form approximate hexagonal close-packed arrays normal to the *a*-axis; one-half of the octahedral interstices are occupied by *M* site atoms and one-eighth of the tetrahedral interstices are occupied by Si. The structure has been discussed in great detail by various workers (Hanke, 1965; Birle *et al,* 1968; Kamb, 1968; Baur, 1972). There are two crystallographi-

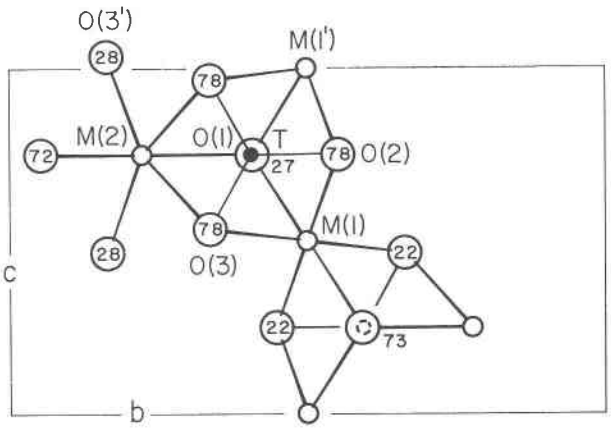

FIG. 1. M site environments in fayalite; M atoms, small open circles; oxygen, large open circles with x coordinates ($\times$ 100); Si, small full circles.

cally distinct M sites: $M(1)$, point symmetry $\bar{1}$; and $M(2)$, point symmetry m. The coordination octahedron of $M(1)$-site atoms (Fig. 1) shares six edges, two with $M(1)$ octahedra, two with $M(2)$ octahedra, and two with Si tetrahedra. The coordination octahedron of $M(2)$-site atoms shares three edges, two with $M(1)$ octahedra and one with a Si tetrahedron. In both octahedra, the shared edges are associated to form octahedral faces which contribute to the "empty" tetrahedron of oxygen atoms (Hanke, 1965; Kamb, 1968). The distortions from ideal octahedral symmetry result from accommodation of the tetrahedral edges and internuclear repulsion associated with all of the shared edges. The $M(1)$ octahedron is stretched as a result of the repulsive forces along one "trigonal" axis. The $M(2)$ atom is displaced away from the octahedral face formed of shared edges. Mg and Fe^{2+} are generally disordered among the $M(1)$ and $M(2)$ sites in all compositions in the forsterite (Fo)—fayalite (Fa) series. The X-ray diffraction study of Birle *et al* (1968) did not detect any M site ordering, and the site ordering reported by other investigators —for example, Finger (1969/1970), Wenk and Raymond (1973), Brown and Prewitt (1973)—is slight.

The present study has been made using the crystal structure data of Birle *et al* (1968) for four olivines, forsterite ($Mg_{0.90}Fe_{0.10}SiO_4$), hyalosiderite ($Mg_{0.535}Fe_{0.456}Mn_{0.006}Ca_{0.002}SiO_4$), hortonolite ($Mg_{0.49}Fe_{0.49}Mn_{0.01}Ca_{0.01}SiO_4$), and fayalite ($Fe_{0.92}Mg_{0.04}SiO_4$). The polyhedral edge-related M–M distances (Birle *et al*, 1968) and M–Si distances and the associated enclosing O–M–O bond angles for M–M interactions and O–Si–O bond angles are given in Table 2. The deviations of the non-equivalent M–O bond distances from the mean M–O distances for each site are given in Table 3.

In the olivine structure, the dominant cohesive forces are the Si–O and M–O bonds. The ideal structure based on hexagonal close-packed arrays of oxygen atoms must distort to allow adjustment of these bond lengths to equilibrium values. The principal distortion in the structure is contraction of the Si–O tetrahedra (Kamb, 1968). Further structural stabilization results through increased separation of the M atoms, away from the shared coordination polyhedra edges (Kamb, 1968; Baur, 1972). This is accompanied by shortening of the O–O distances along the shared edges, which allows greater M–M and M–Si separations without undue stretching of the M–O and Si–O bonds. In the present study O–M–O and O–Si–O bond angles are used, where applicable, as measurements of relative stretching of M–M and M–Si distances rather than the associated shared-edge lengths. Although the latter are related to the repulsive forces involved, they are also affected by other factors, for example, size of the coordinated metal

TABLE 2. Edge-Related Interatomic Distances (Å) and Associated Bond Angles (°) in Olivines

	Forsterite ($Fo_{90.0}$)	Hyalosiderite ($Fo_{53.5}$)	Hortonolite ($Fo_{49.0}$)	Fayalite ($Fo_{4.0}$)
M(1)-M(1')	2.997	3.019	3.022	3.050
O(1)-M(1)-O(2)	86.60	86.60	86.47	86.38
M(1)-M(2)	3.209	3.251	3.259	3.305
O(1)-M(1)-O(3)	84.86	84.49	84.80	84.60
O(1)-M(2)-O(3)	81.10	81.04	80.53	80.69
M(1)-Si	2.704	2.731	2.734	2.768
O(3)-Si-O(2)	102.01	102.09	102.61	103.00
M(2)-Si	2.800	2.838	2.841	2.872
O(3)-Si-O(3)	104.51	105.59	105.63	105.57

TABLE 3. Deviations (%) of M–O Bond Distances from Mean Values (Å) in Olivines

	Forsterite ($Fo_{90.0}$)	Hyalosiderite ($Fo_{53.5}$)	Hortonolite ($Fo_{49.0}$)	Fayalite ($Fo_{4.0}$)
M(1)-O(1)	-0.6	-0.5	-1.4	-1.6
-O(2)	-1.3	-1.7	-1.2	-1.7
-O(3)	+1.9	+2.2	+2.5	+3.2
⟨M(1)-O⟩	2.103	2.127	2.129	2.159
M(2)-O(1)	+2.0	+1.2	+2.2	+2.5
-O(2)	-3.6	-2.9	-3.9	-3.1
-O(3)	+3.8	+5.1	+5.3	+5.2
-O(3')	-3.0	-4.3	-4.4	-4.9
⟨M(2)-O⟩	2.135	2.152	2.154	2.178

atoms. The preceding discussion implies that the Si atoms experience repulsion from the M atoms related through shared edges; this is supported by relatively small O–Si–O bond angles (and relatively short O–O distances).

The repulsive M–M and M–Si interactions leave the $M(1)$ atom in the center of its coordination octahedron. All of the $M(1)$–O distances are stretched by these repulsive interactions and, in general, the distortions tend to be constrained by the structure as a whole so as to be partially suppressed. In contrast, an $M(2)$ atom may respond to repulsion due to edge-related atoms by displacement away from the shared edges. In the fayalite of Birle *et al* (1968) the mean $M(2)$–O distances for shared and unshared edges are 2.27 Å and 2.08 Å, respectively; the difference (0.19 Å) must largely reflect the repulsion resulting from the edge-related Si and $M(1)$ atoms. Thus, the destabilization resulting from these repulsions is quite considerable. Variations in the individual $M(2)$–O bond lengths may be used directly to estimate the relative repulsion experienced by various pairs of cations. For the four olivine compositions used (Table 2), the deviations in $M(2)$–$O(3)$ distances are appreciably greater than those in $M(2)$–$O(1)$ distances, so that $M(2)$–Si repulsion is greater than $M(2)$–$M(1)$ repulsion. However, this may largely reflect the shorter ideal $M(2)$–Si distance and cannot be used to infer that the charge on a Si atom is greater than that on either Mg or Fe^{2+} atoms. The data in Table 2 do suggest, though, that the distortions of both $M(1)$ and $M(2)$ octahedra are greatest in fayalite and that Fe^{2+}–Si repulsion is greater than Mg–Si repulsion and Fe^{2+}–Fe^{2+} repulsion is greater than Mg–Mg repulsion, which is contrary to the predictions made in the introduction. Of course, this discrepancy may result because accommodation of the larger Fe^{2+} atoms may make the structure more susceptible to interatomic repulsive forces.

The mean M–O distances and the edge-related M–M and $M(1)$–Si distances show linear variations with Fo content, which are expected from the known linear variations of the unit cell parameters of olivines with composition and are evidence in favor of ideal solution. However, the individual M–O bonds (Table 3), the edge-related $M(2)$–Si distances (Fig. 2), and the O–M–O and O–Si–O angles associated with the shared edges (Table 2) indicate slight departures from the trends expected for ideal solution. Clearly, the adjustments made by the olivine structure to accommodate Fe^{2+} atoms are more complex than those attributable to merely a gradual increase in the size of the unit cell. However, the variations in the M–M and M–Si distances with composition are not consistent with possible neutralization of the nuclear charge on Fe^{2+} by the $3d$ electrons in the t_{2g} orbitals projecting along M–M vectors. Although it cannot be concluded from the data available that the departures from ideal behavior are not due to occupied t_{2g} orbitals on Fe^{2+}, it is rather surprising to observe that these orbitals do not screen the nuclear charge on Fe^{2+}.

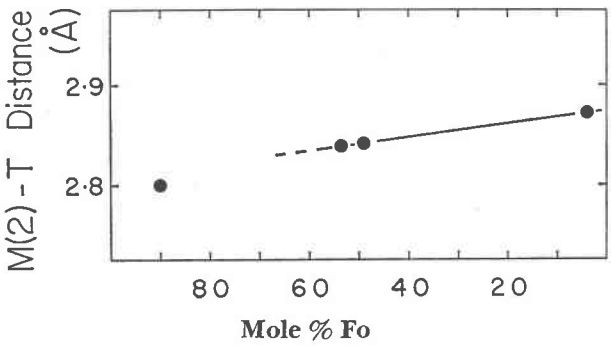

FIG. 2. Variation of $M(2)$–Si distances in olivines with forsterite content.

Clinopyroxenes

The compilation of crystal structure data for $C2/c$ clinopyroxenes of Clark, Appleman, and Papike (1969) represents a wide variety of end member compositions and includes data for jadeite ($NaAlSi_2O_6$, Prewitt and Burnham, 1966), $NaIn^{3+}Si_2O_6$ (Christensen and Hazell, 1967), johannsenite ($CaMn^{2+}Si_2O_6$, Freed and Peacor, 1967), and spodumene ($LiAlSi_2O_6$), $LiFe^{3+}Si_2O_6$, ureyite ($NaCr^{3+}Si_2O_6$), acmite ($NaFe^{3+}Si_2O_6$), and diopside ($CaMgSi_2O_6$). The Li clinopyroxenes have the probable space group $C2$ but were refined in $C2/c$ to obtain average structures. The data for these eight clinopyroxenes are the basis of the present study.

In the $C2/c$ clinopyroxene structure, single chains of Si–O tetrahedra are parallel to the c axis. The two crystallographically distinct M sites are arranged in planes parallel to (100) at $x = 0, 1/2$. The smaller $M(1)$ coordination octahedron (Fig. 3) is formed entirely of six non-bridging tetrahedral oxygens. Although the point symmetry of the $M(1)$ site is 2, the distortions of the $M(1)$ octahedron from ideal sym-

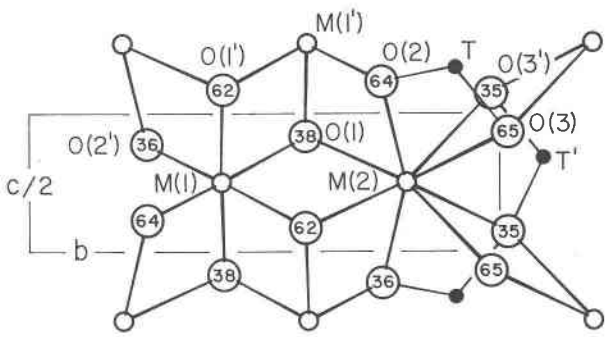

FIG. 3. M site environments in diopside; M atoms, small open circles; oxygen, large open circles with x coordinates ($\times$ 100); T atoms (Si), small full circles.

metry are not very great. The $M(1)$ octahedron has five shared edges, two with $M(1)$ octahedra and three with $M(2)$ polyhedra. The larger $M(2)$ coordination polyhedron is formed of both bridging and non-bridging oxygens. The bridging oxygens all lie to one side of the plane parallel to (010) passing through the $M(2)$ atom, and the $M(2)$ atom is generally displaced towards the non-bridging oxygens. In Na and Ca clinopyroxenes, the $M(2)$ atoms are eight-fold coordinated and the $M(2)$ polyhedron is quite irregular. It shares three edges with $M(1)$ octahedra, two with $M(2)$ polyhedra, and three with T tetrahedra, although the two $M(2)$–$M(2)$ interactions and the $M(2)$–T' interaction involve long $M(2)$–O(3′) distances and the resulting repulsive forces between these juxtaposed cations must be minimal. Distortions in the $M(2)$ polyhedron then arise, in part, through accommodation of shorter shared tetrahedral and $M(1)$ octahedral edges and shorter bonds to non-bridging oxygens. Repulsion between edge-related atoms must contribute to the distortion in both $M(1)$ and $M(2)$ polyhedra. In addition, Clark, Appleman, and Papike (1969) have noted that the shortest bonded distances from T, $M(1)$, and $M(2)$ atoms are all to O(2) atoms. O(2) is coordinated to only three atoms, and apparently the additional bonding is shared among these. In terms of the ionic bonding model, the extra negative electrostatic valence is compensated by extra positive

TABLE 4. Edge-Related Interatomic Distances, Associated Bond Angles, and Deviations from Mean Values of M–O Bond Distances in $C2/c$ Clinopyroxenes

	LiAl	$LiFe^{3+}$	NaAl	$NaCr^{3+}$	$NaFe^{3+}$	NaIn	CaMg	$CaMn^{2+}$
Selected Edge-Related Interatomic Distances (Å) and Associated Bond Angles (°) in C2/c Clinopyroxenes								
M(1)-M(1)	3.042	3.177	3.066	3.089	3.189	3.302	3.092	3.164
O(1)-M(1)-O(1')	78.9	80.9	77.4	80.6	79.2	81.78	84.6	87.7
M(1')-M(2)	3.020	3.018	3.154	3.201	3.172	3.239	3.221	3.256
M(1)-M(2)	3.091	3.206	3.381	3.426	3.527	3.731	3.500	3.631
O(1)-M(1)-O(1)	84.8	81.9	86.2	85.8	83.1	80.15	82.2	79.2
M(2)-T	2.862	2.911	2.982	3.000	3.028	3.046	3.102	3.126
O(2)-T-O(3)	104.2	104.6	105.9	106.1	105.6	106.7	103.46	103.80
M(2)-T'	3.309	3.427	3.168	3.205	3.238	3.307	3.312	3.388
O(3)-T'-O(3')	107.3	108.9	106.3	107.1	107.1	109.55	104.17	104.71
Deviations (%) of M-O Bond Distances from Mean Values (Å) in C2/c Clinopyroxenes								
M(1)-O(1)	+4.1	+5.3	+3.5	+2.1	+4.1	+3.2	+1.8	+2.7
-O(1')	+1.3	+0.1	+0.3	+0.6	+0.2	+0.7	-0.6	-0.8
-O(2')	-5.3	-5.4	-3.7	-2.6	-4.4	-4.0	-1.3	-1.8
⟨M(1)-O⟩	1.919	2.031	1.928	1.998	2.025	2.142	2.077	2.173
M(2)-O(1)	-4.8	-5.7	-0.9	-0.8	-0.7	-0.9	-2.7	-2.7
-O(2)	+3.0	-3.6	+1.5	-0.3	0.0	-2.8	-3.0	-5.5
-O(3)	+1.8	+9.3	-0.6	+1.1	-0.7	+2.1	+5.6	+8.2
-O(3')	+42.2	+41.3	+15.3	+15.3	+17.3	+18.5	+12.0	+13.1
⟨M(2)-O⟩*	2.211	2.249	2.378	2.397	2.414	2.466	2.425	2.450

* Mean of six nearest oxygens

electrostatic valence on the adjacent cations. In a covalent bonding model the O(2) atom could form σ bonds with distorted sp^2 triangular hybrid orbitals, and the extra bonding could be contributed through π bonds between the p_z orbital on O(2) and orbitals on the adjacent atoms.

Selected edge-related M–M and M–T distances and associated enclosing O–$M(1)$–O and O–T–O bond angles are given in Table 4; the $M(1)$–$M(1)$ distances and all of the bond angles are from Clark, Appleman, and Papike (1969).

The deviations of the non-equivalent M–O distances from the mean M–O bond distances for both $M(1)$ and $M(2)$ atoms are given in Table 4; the data for $M(2)$ atoms are relative to the six shortest $M(2)$–O distances to allow realistic comparisons with the Li clinopyroxene data.

The problem of associating specific distortions in coordination polyhedra with the repulsive forces between individual pairs of cations is more difficult for clinopyroxenes than for olivines because of the greater complexity of the clinopyroxene structure. In particular, the Si–O tetrahedra may not move independently of one another, and there appears to be a large variation in $M(2)$–O bond strengths. Moreover, the data for deviations in the $M(1)$–O(2) bonds and, to a lesser extent, in the $M(1)$–O(1) bonds (Table 4) do suggest a certain amount of $M(2)$ control on the configuration of the $M(1)$ octahedron. However, the data for the deviations in the $M(2)$–O bond distances (Table 4) do not show systematic correlations between those pyroxenes with common $M(1)$ atoms, and it appears that the $M(2)$ polyhedron configuration is largely independent of the $M(1)$ atom.

The deviations in the $M(2)$–O(3) bond distances and the variations in the O(2)–T–O(3) bond angles do suggest that the $M(2)$–Si repulsion varies systematically with the type of $M(2)$ atom and decreases in the sequence Ca–Si > Li–Si > Na–Si, in agreement with the predictions made in the introduction.

The O(1)–$M(1)$–O(1) bond angles are appreciably less than 90° and decrease fairly systematically with $M(1)$–$M(2)$ distance (Fig. 4). However, the closest approach of $M(1)$ and $M(2)$ atoms is really defined by the $M(1')$-$M(2)$ distances (Fig. 5), and the acute angles result, in part, because the $M(1)$ atom is drawn by the multiple bonding toward the O(2) atoms on the opposite side of the $M(1)$ octahedron. Also, repulsion between $M(1)$ and

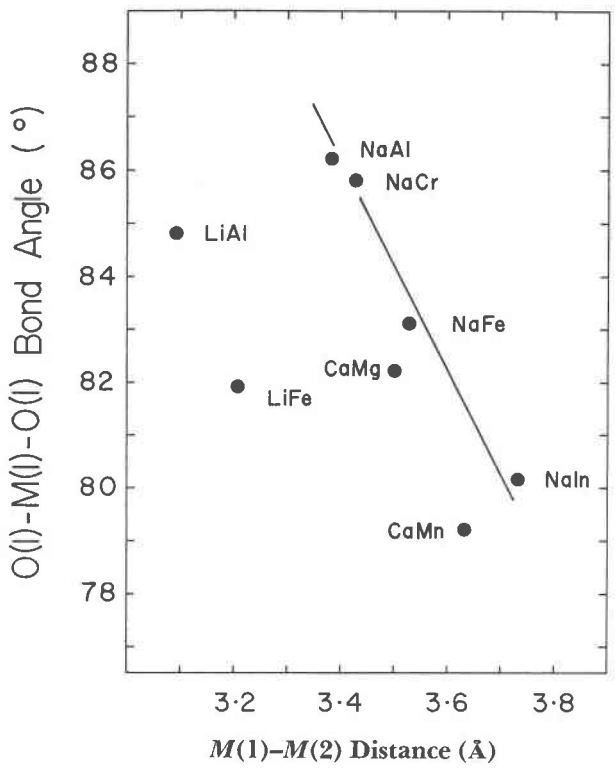

FIG. 4. Variation of O(1)–$M(1)$–O(1) bond angle in $C2/c$ clinopyroxenes with $M(1)$–$M(2)$ distance.

$M(2)$ atoms cannot be too significant since both $M(1')$–$M(2)$ and $M(1)$–$M(2)$ distances increase more or less proportionally to the sums of the ionic radii of the $M(1)$ and $M(2)$ cations.

The O(1)–$M(1)$–O(1′) bond angle varies with the type of $M(1)$ atom (Table 4), suggesting that $M(1)$–$M(1)$ repulsion decreases in the sequence: Al > Fe^{3+} ≃ Cr^{3+} > In > Mg > Mn^{2+}. Distortion due to $M(1)$–$M(1)$ repulsion is illustrated in plots of $M(1)$–$M(1')$ against mean $M(1)$–O bond distance (Fig. 6). The relative stretching of the $M(1)$–$M(1')$ distances suggests that $M(1)$–$M(1)$ repulsion decreases in the sequence Al > Fe^{3+} > In > Cr^{3+} ≫ Mg > Mn^{2+}. These sequences are fairly consistent with the data in Table 1.

The $M(1)$ atoms include a variety of group II and III elements and 3d transition metals. Once again there is no evidence that occupied t_{2g} orbitals on the transition metals (Cr^{3+}, Fe^{3+}, and Mn^{2+}) perturb the coordination polyhedra containing them, and it appears that electrons in these orbitals do not screen the nuclear charge very efficiently along M–M directions.

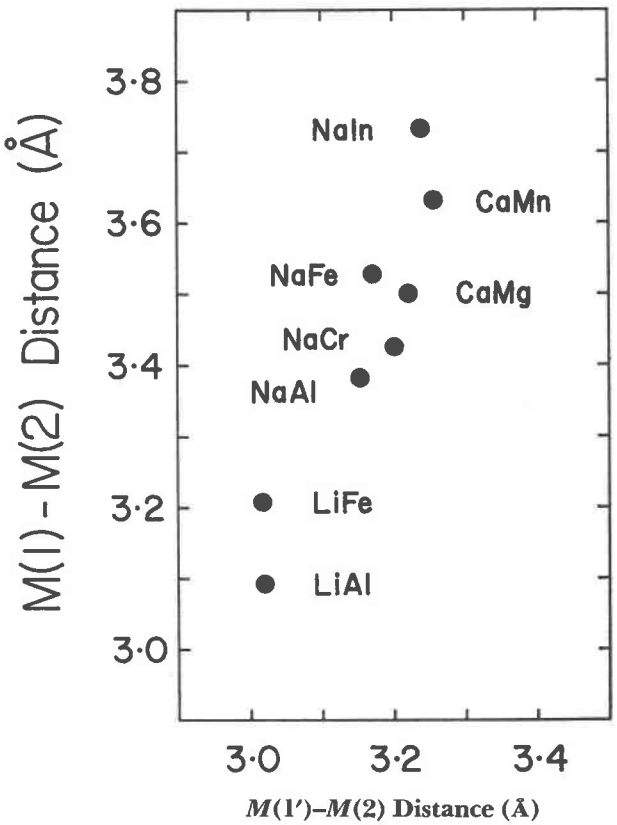

FIG. 5. Variation of $M(1)$–$M(2)$ distance in $C2/c$ clinopyroxenes with $M(1')$–$M(2)$ distance.

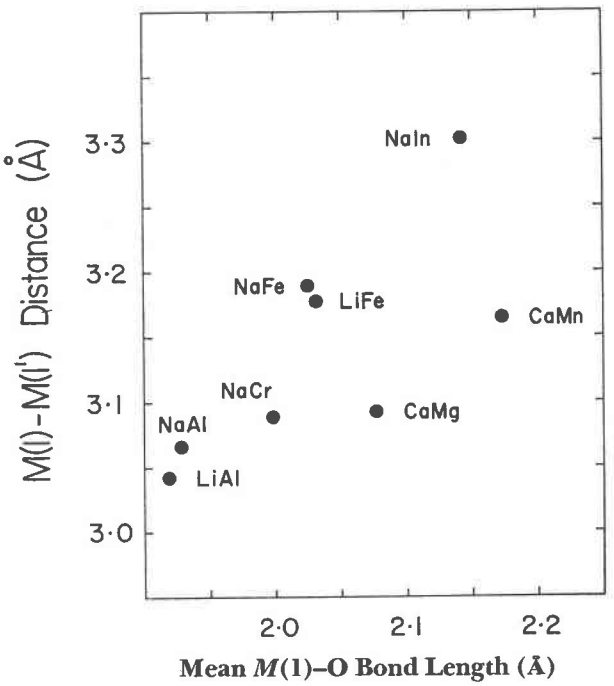

FIG. 6. Variation of $M(1)$–$M(1')$ distance in $C2/c$ clinopyroxenes with mean $M(1)$–O bond length.

Amphiboles

The amphibole minerals are complex chemically, and while a great deal of crystal structure work has been done on them there is insufficient data to allow a worthwhile comparison of edge-related distortions in either ideal end-member compositions or in representatives of a single solid solution series. However, structural refinements have been made on three (Ca),Mg,Fe^{2+} amphiboles, tremolite (Papike, Ross, and Clark, 1969), actinolite (Mitchell, Bloss, and Gibbs, 1971), and grunerite (Finger, 1969), and a preliminary study on the sites effectively dominated by Mg and Fe^{2+} may be mentioned.

The tremolite structure consists of double chains, or bands, of Si–O tetrahedra parallel to the c axis with the four non-equivalent M sites (Fig. 7) arranged in strips parallel to (100). The $M(4)$ atom coordination polyhedron is essentially equivalent in almost all structural details to the $M(2)$ polyhedron in clinopyroxene, but it is occupied by Ca in the tremolite studied, by Ca(Na) in the actinolite and by Fe^{2+}(Mg) in the grunerite so that realistic comparisons of distortions within these polyhedra cannot be made. The $M(1)$, $M(2)$, and $M(3)$ octahedra (Fig. 7) are all approximately equivalent to the $M(1)$ octahedron in clinopyroxene, being only slightly distorted and formed of non-bridging oxygens, although $(OH)^-$ groups do contribute to the $M(1)$ and $M(3)$ octahedra. The $M(1)$ site has point symmetry 2: the $M(1)$ octahedron shares six octahedral

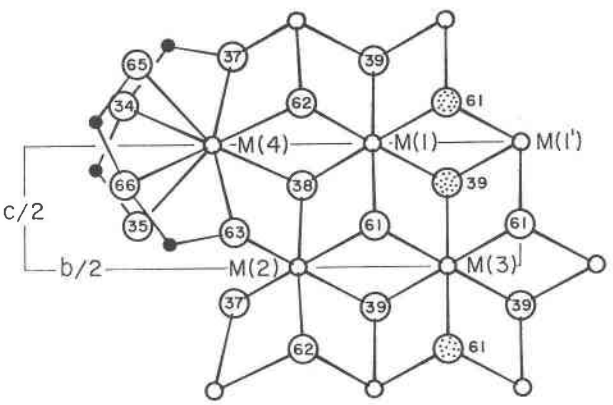

FIG. 7. M site environments in tremolite; M atoms, small open circles; oxygen, large open circles with x coordinates (× 100); hydroxyl groups, stippled; T atoms, small full circles.

edges, two with $M(2)$ and $M(3)$ octahedra and one each with a $M(1)$ octahedron and a $M(4)$ polyhedron. The $M(2)$ site has point symmetry 2 also; the $M(2)$ polyhedron shares five octahedral edges, two with $M(1)$ octahedra, two with $M(4)$ polyhedra, and one with a $M(3)$ octahedron. The $M(3)$ site has point symmetry $2/m$; the $M(3)$ octahedron shares six octahedral edges, four with $M(1)$ octahedra and two with $M(2)$ octahedra. The O–*M*–O bond angles associated with shared edges are all significantly less than 90° and, as a result of the repulsion between the edge-related *M* site atoms, the $M(1)$, $M(2)$, and $M(3)$ octahedra are compressed parallel to [100], each being essentially trigonally distorted.

When the edge-related *M*–*M* distances are plotted against mean *M*–O bond lengths (Fig. 8), certain structural controls on the polyhedral distortions are quite evident. In particular, the *M*–*M* distances parallel to the *b* axis ($M(1)$–$M(1')$, $M(1)$–$M(4)$, and $M(2)$–$M(3)$) are stretched the most and must reflect the relative rigidity of the Si–O tetrahedral bands along their lengths (parallel to the *c* axis). Also, the $M(1)$–$M(1')$ distance is dependent on the nature of the $M(4)$ cation but the $M(1)$–$M(2)$, $M(1)$–$M(3)$, and $M(2)$–$M(3)$ distances appear not to be. However, the data do show the expected general increase in size of coordination polyhedra with increase in Fe^{2+} content. In the Ca amphiboles, though, the $M(1)$–$M(4)$ and $M(2)$–$M(4)$ distances do not increase with Fe^{2+} content; one may conclude, tentatively, that electrostatic repulsion from Mg exceeds that from Fe^{2+} in these minerals.

Conclusions

The apparent magnitudes of the $M(1)$–$M(1)$ and $M(2)$–Si repulsions of edge-related coordination polyhedra in $C2/c$ clinopyroxenes show partial correlation with the electrostatic potentials due to the *M* atoms calculated from electronegativity data. The principal exception to this relates to the electrostatic potentials calculated for Fe^{3+} in $LiFeSi_2O_6$ and acmite ($NaFeSi_2O_6$) and for Cr^{3+} in ureyite ($NaCrSi_2O_6$); when the O(1)–$M(1)$–O(1′) bond angle is plotted against electrostatic potentials calculated from both electronegativity and positron Z_{eff} data (Fig. 9) the correlation is substantially improved.

The *M*–*M* repulsive distortions in (Ca),Mg,Fe^{2+} amphiboles tend to be constrained by the double chains of Si–O tetrahedra. However, in Ca amphiboles, $M(1)$–Ca and $M(2)$–Ca distances do suggest, in agreement with the calculated data, that the elec-

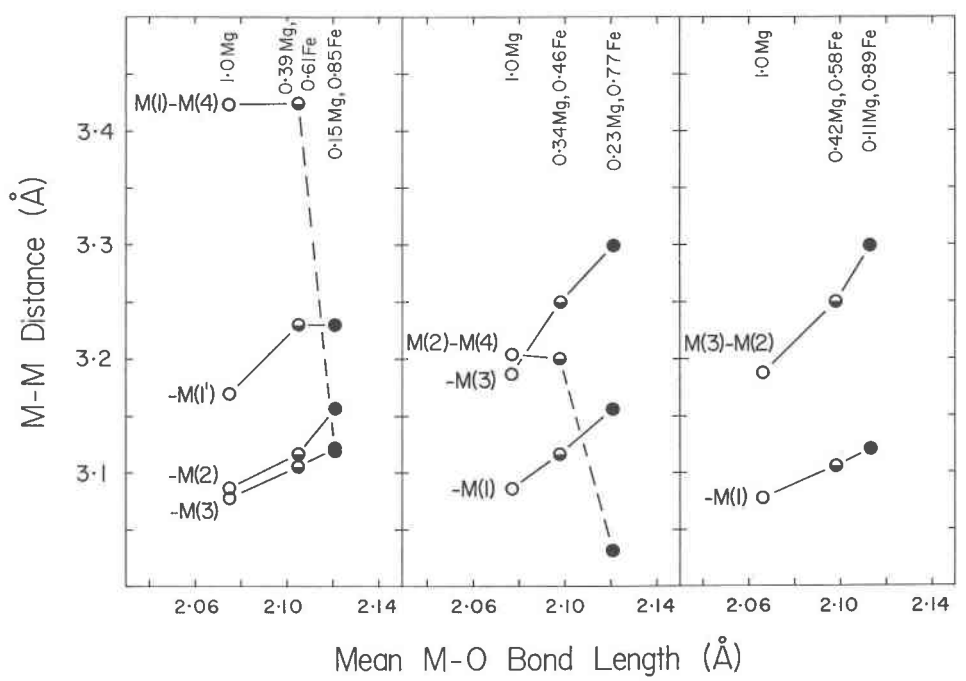

FIG. 8. Variation of *M*–*M* distance with *M*–O bond length for $M(1)$, $M(2)$, and $M(3)$ sites of (Ca),Mg,Fe^{2+} amphiboles; tremolite, open circles; actinolite, half-open circles; grunerite, full circles; Mg and Fe^{2+} data refer to individual site occupancies.

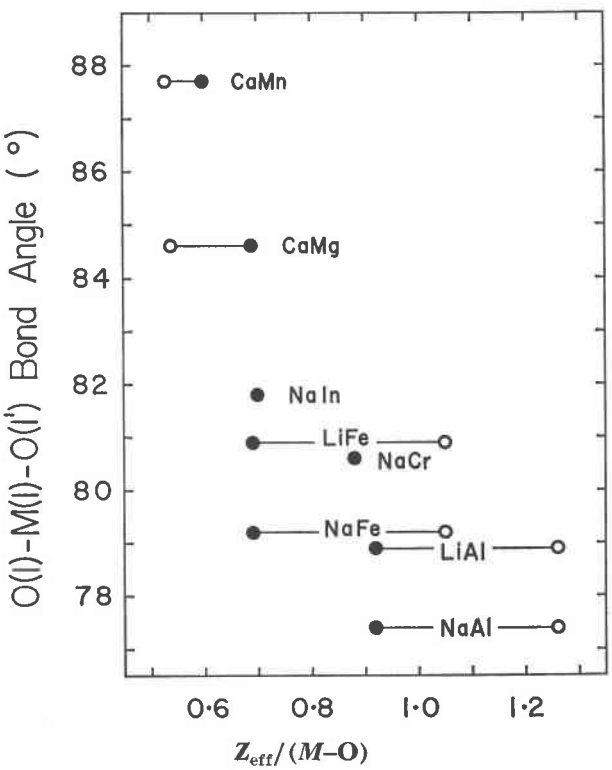

FIG. 9. Variation of O(1)–M(1)–O(1′) bond angle in $C2/c$ clinopyroxenes with electrostatic potential, $Z_{eff}/(M–O)$ calculated from electronegativity data (solid circles) and positron method data (open circles).

trostatic potential due to Mg is apparently greater than that due to Fe^{2+}. In contrast, in olivines, distortions related to both M-M and M-Si repulsive interactions indicate that the repulsion due to Fe^{2+} is greater than that due to Mg.

Quantitative comparisons between M–M and M–T distortions and calculated electrostatic potentials have not been attempted in this study because of the uncertainty in the calculated potentials and the difficulty in isolating the effects of specific distorting forces in complex structures. For example, in clinopyroxenes it has been noted that there is some $M(2)$ atom control on the distortions of the $M(1)$ atom octahedron. It is expected that $M(1')$–$M(2)$ repulsions will tend to negate the effects of $M(1)$–$M(1')$ repulsions (Fig. 3) and that this tendency will decrease in the $M(2)$ site occupancy sequence Ca > Li > Na: this is largely confirmed in plots of the O(1)–M(1)–O(1′) bond angle against $Z_{eff}/(M–O)$ (Fig. 9).

However, the present approach does demonstrate that, for olivines and $C/2c$ clinopyroxenes, 3d electrons in t_{2g} orbitals do not appear to screen the effective atomic charges of transition metal atoms along M–M and M–Si directions.

Acknowledgments

This work was supported by a National Research Council of Canada operating grant.

References

BARTENEV, G. M., A. Z. VARISOV, V. I. GOLDANSKII, E. P. PROKOPEV, AND A. D. TSYGANOV (1972) Determination of the effective charges of anions in media of the ionic type by the positron method. *Russ. Chem. Rev.* **41,** 305–313.

BATSANOV, S. S. (1968) The concept of electronegativity. Conclusions and prospects. *Russ. Chem. Rev.* **37,** 332–351.

BAUR, W. H. (1970) Bond length variation and distorted coordination polyhedra in inorganic crystals. *Trans. Am. Crystallogr. Assoc.* **6,** 129–155.

——— (1972) Computer-simulated crystal structures of observed and hypothetical Mg_2SiO_4 polymorphs of low and high density. *Am. Mineral.* **57,** 709–731.

BIRLE, J. D., G. V. GIBBS, P. B. MOORE, AND J. V. SMITH (1968) Crystal structures of natural olivines. *Am. Mineral.* **53,** 807–824.

BROSTIGEN, G., AND A. KJEKSHUS (1970) Bonding schemes for compounds with the pyrite, marcasite, and arsenopyrite type structures. *Acta Chem. Scand.* **24,** 2993–3012.

BROWN, G. E., AND C. T. PREWITT (1973) High-temperature crystal chemistry of hortonolite. *Am. Mineral.* **58,** 577–587.

BROWN, I. D., AND R. D. SHANNON (1973) Empirical bond-strength bond-length curves for oxides. *Acta Crystallogr.* **A29,** 266–282.

BURNS, R. G. (1970) *Mineralogical Applications of Crystal Field Theory*. Cambridge University Press, Cambridge, United Kingdom.

CHRISTENSEN, A. N., AND R. G. HAZELL (1967) The crystal structure of $NaIn(SiO_3)_2$. *Acta Chem. Scand.* **21,** 1425–1429.

CLARK, J. R., D. E. APPLEMAN, AND J. J. PAPIKE (1969) Crystal-chemical characterization of clinopyroxenes based on eight new structure refinements. *Mineral. Soc. Am. Spec. Pap.* **2,** 31–50.

COCHRAN, W. (1961) "Effective" ionic charge in crystals. *Nature,* **191,** 60–61.

COPPENS, P. (1972) Alternatives in the comparison of theoretical and experimental charge densities: Difference maps, net atomic charges, and population parameters. *Trans. Am. Crystallogr. Assoc.* **8,** 93–111.

FINGER, L. W. (1969) The crystal structure and cation distribution of a grunerite. *Mineral. Soc. Am. Spec. Pap.* **2,** 95–100.

——— (1969/1970) Fe/Mg ordering in olivines. *Carnegie Inst. Wash. Year Book,* **69,** 302–305.

FLEET, M. E. (1973) The crystal structure of maucherite ($Ni_{11}As_8$). *Am. Mineral.* **58,** 203–210.

FREED, R. L., AND D. R. PEACOR (1967) Refinement of the crystal structure of johannsenite. *Am. Mineral.* **52,** 709–720.

GIBBS, G. V., M. M. HAMIL, L. S. BARTELL, AND H. YOW (1972) Correlations between Si-O bond length, Si-O-Si angle, and bond overlap populations calculated using extended Hückel molecular orbital theory. *Am. Mineral.* **57,** 1578–1613.

HANKE, K. (1965) Beiträge zu kristallstrukturen vom Olivin-Typ. *Beitr. Mineral. Petrogr.* **11,** 535–558.

KAMB, B. (1968) Structural basis of the olivine-spinel stability relation. *Am. Mineral.* **53,** 1439–1455.

LOUISNATHAN, S. J., AND G. V. GIBBS (1972a) The effect of tetrahedral angles on Si-O bond overlap populations for isolated tetrahedra. *Am. Mineral.* **57,** 1614–1642.

———, AND ——— (1972b) Variation of Si-O distances in olivines, soda melilite, and sodium metasilicate as predicted by semi-empirical molecular orbital calculations. *Am. Mineral.* **57,** 1643–1663.

MITCHELL, J. T., F. D. BLOSS, AND G. V. GIBBS (1971) Examination of the actinolite structure and four other *C2/m* amphiboles in terms of double bonding. *Z. Kristallogr.* **133,** 273–300.

NICKEL, E. H. (1968) Structural stability of minerals with the pyrite, marcasite, arsenopyrite, and löllingite structures. *Can. Mineral.* **9,** 311–321.

PAPIKE, J. J., M. ROSS, AND J. R. CLARK (1969) Crystal-chemical characterization of clinoamphiboles based on five new structure refinements. *Mineral. Soc. Am. Spec. Pap.* **2,** 117–136.

PAULING, L. (1929) The principles determining the structure of complex ionic crystals. *J. Am. Chem. Soc.* **51,** 1010–1026.

——— (1960) *The Nature of the Chemical Bond,* 3rd. ed. Cornell University Press, Ithaca, New York.

PEARSON, W. B. (1965) Compounds with the marcasite structure. *Z. Kristallogr.* **121,** 449–462.

PREWITT, C. T., AND C. W. BURNHAM (1966) The crystal structure of jadeite, $NaAlSi_2O_6$. *Am. Mineral.* **51,** 956–975.

ROBINSON, K., G. V. GIBBS, AND P. H. RIBBE (1971) Quadratic elongation: A quantitative measure of distortion in coordination polyhedra. *Science,* **172,** 567–570.

SEIGBAHN, K., C. NORDLING, A. FAHLMAN, R. NORDBERG, K. HAMRIN, J. HEDMAN, G. JOHANSSON, T. BERGMARK, S.-E. KARLSSON, I. LINDGREN, AND B. LINDBERG (1967) ESCA, atomic, molecular and solid state structure studied by means of electron spectroscopy. *Nova Acta Regiae Soc. Sci. Upsaliensis, Ser. IV,* Vol. **20.**

SHANNON, R. D., AND C. T. PREWITT (1969) Effective ionic radii in oxides and fluorides. *Acta Crystallogr.* **B25,** 925–946.

TOSSELL, J. A. (1973) Interpretation of *K* X-ray emission spectra and chemical bonding in oxides of Mg, Al, and Si using quantitative molecular orbital theory. *Geochim. Cosmochim. Acta,* **37,** 583–594.

URUSOV, V. S. (1967) Chemical bonding in silica and silicates. *Geochem. Int.* **4,** 350–362.

WENK, H.-R., AND K. N. RAYMOND (1973) Four new structure refinements of olivine. *Z. Kristallogr.* **137,** 86–105.

Manuscript received, August 13, 1973; accepted for publication, April 24, 1974.